energies

MDPI

Article

Advanced Spectral Diagnostics of Jet Engine Vibrations Using Non-Contact Laser Vibrometry and Fourier Methods

Wojciech Prokopowicz [1], Bartosz Ciupek [2,*], Artur Maciąg [3], Tomasz Gajewski [4] and Piotr Witold Sielicki [4]

[1] Ministry of National Defense, 00-911 Warsaw, Poland; wojtek379379@gmail.com
[2] Department of Fuels and Renewable Energy, Faculty of Environmental Engineering and Energy, Institute of Thermal Energy, Poznan University of Technology, 60-965 Poznan, Poland
[3] Faculty of Management and Computer Modelling, Kielce University of Technology, 25-314 Kielce, Poland; matam@tu.kielce.pl
[4] Faculty of Civil and Transport Engineering, Institute of Structural Analysis, Poznan University of Technology, 60-965 Poznan, Poland; tomasz.gajewski@put.poznan.pl (T.G.); piotr.sielicki@put.poznan.pl (P.W.S.)
* Correspondence: bartosz.ciupek@put.poznan.pl

Abstract

This study presents an advanced diagnostic methodology for assessing mechanical faults in high-performance jet engines using non-contact laser vibrometry and Fourier-based vi-bration analysis. Focusing on Pratt & Whitney F100-PW-229 engines used in F-16 aircraft, thise research identifies critical measurement locations, including the gearbox, turbine, and compressor supports. High-resolution vibration signals were collected under test bench conditions and processed using fFast Fourier tTransform (FFT) techniques to extract frequency-domain features indicative of rotor imbalances, bearing wear, and structural anomalies. Comparative analysis between nominal and degraded engines confirmed strong correlations between analytical predictions and empirical spectral patterns. Thise study introduces a signal processing framework combining time–frequency analysis with Relief-F-based feature selection, laying the groundwork for future integration with ma-chine learning algorithms. This non-intrusive, efficient diagnostic method supports early fault detection, enhances engine availability, and contributes to the development of a na-tional vibration reference database, especially vital in the absence of OEM-supplied tools.

Keywords: jet engine diagnostics; vibration analysis; Fourier transform; laser vibrometry; non-contact measurement; signal processing; bearing damage detection

Academic Editors: Silvia Ravelli, Juana María Martínez-Heredia and Francisco Colodro Ruiz

Received: 10 July 2025
Revised: 8 September 2025
Accepted: 8 September 2025
Published: 11 September 2025

Citation: Prokopowicz, W.; Ciupek, B.; Maciąg, A.; Gajewski, T.; Sielicki, P.W. Advanced Spectral Diagnostics of Jet Engine Vibrations Using Non-Contact Laser Vibrometry and Fourier Methods. *Energies* **2025**, *18*, 4837. https://doi.org/10.3390/en18184837

1. Introduction

Throughout the service life of an aircraft engine, vibrations of individual components and the entire engine module serve as critical diagnostic indicators. These vibrations may result from various engine-related processes that influence the propulsion system during both airborne operation and ground testing. Typically, vibration data are collected using accelerometers mounted directly on components of interest. However, the use of such instrumentation increases system complexity and introduces technical challenges, especially in confined engine environments. Moreover, the number of potential measurement points is limited by the physical locations where accelerometers can be installed.

Vibrations in aircraft engines are primarily caused by the mass and stiffness properties of rotating parts and the structural connection between the engine and the airframe. The vibration amplitude depends largely on mechanical factors such as mass distribution,

moment of inertia, balance quality, support methods for rotating components, material elasticity and damping characteristics, and the geometry of engine assemblies [1].

In addition to vibrations generated by the engine itself, the vibration spectrum may include signals from other aircraft systems, particularly those originating in the airframe. The overall vibration intensity is influenced by flight conditions, pilot operation, and external environmental factors.

Measuring vibration allows for the assessment of alternating stresses that lead to fatigue and damage in internal engine components. During engine operation, changes in the mass and stiffness distribution of rotating parts may occur, causing variations in the forces transmitted to adjacent assemblies. The recorded vibration signal contains valuable information about these dynamic forces and reflects the mechanical condition of the engine. For this reason, vibration analysis remains an essential tool in the diagnosis and predictive maintenance of aircraft propulsion systems.

Allouis et al. (2025) [2] investigated the impact of Hydroprocessed Esters and Fatty Acids (HEFA) biofuel on emissions and vibrational characteristics of micro gas turbines (MGTs). Operating under fixed-load conditions, the study demonstrated that replacing JP8 with HEFA significantly reduced CO and particulate emissions, by up to two orders of magnitude. Simultaneously, nonlinear vibrational analysis revealed a critical frequency region ($\omega^* \approx 1.977$ rad) where clustering patterns were distinctly associated with fuel composition. Transitional behavior was particularly evident in the 20–40% HEFA blending range, highlighting the complementary value of integrating emissions monitoring with nonlinear vibration diagnostics for stable and clean combustion in sustainable fuel applications.

Bu et al. (2021) [3] provided a comprehensive review of testing methodologies for aero-engine fan noise, emphasizing the complexity and cost associated with high-fidelity experimental campaigns. The authors highlighted acoustic mode detection and source reconstruction methods as key tools for understanding noise generation mechanisms in rotor-stator configurations. Recent developments based on compressive sensing and machine learning were also reviewed, showcasing their potential to disrupt conventional practices and guide future research directions in aeroacoustic diagnostics for next-generation engines.

Vignat et al. (2024) [4] examined non-ideal effects in a rotating detonation engine (RDE) using large-eddy simulations (LES) and a novel wavenumber-domain filtering technique. This approach allowed for the decomposition of rotating waves and the identification of weak secondary waves and their interactions with detonation fronts. The results showed that these interactions generate precessing high-pressure regions that enhance thrust output via pressure gain combustion. This study contributes new insights into injector response dynamics and introduces a simplified yet effective method for analyzing complex wave modes in detonation-based propulsion systems.

Ahmed et al. (2021) [5] conducted a critical review of failure modes, diagnostics, and acoustic measurement techniques for aircraft auxiliary power units (APUs). Emphasizing the importance of real-time, non-intrusive condition monitoring, the authors discussed vibroacoustic sensors as a viable solution for detecting incipient faults without compromising system integrity. The review synthesized diagnostic methodologies and highlighted the need for innovative signal processing and machine learning tools in the evolving landscape of aircraft health monitoring systems.

Moghadam and Nejad (2021) [6] proposed a theoretical and experimental framework for diagnosing drivetrain faults in wind turbines using torsional vibration measurements and modal parameter estimation. Their method detects deviations in natural frequencies and damping ratios as indicators of structural anomalies. Local sensitivity analysis was employed to relate fault progression to dynamic changes in stiffness and inertia, enabling fault localization without the need for additional instrumentation. The approach was

validated on both simulated and operational drivetrain systems, offering a computationally efficient solution for condition monitoring in floating wind turbines.

Rego et al. (2022) [7] explored jet-installation noise reduction mechanisms using flow-permeable trailing edges. Numerical simulations involving subsonic jets and flat plates with various porous inserts (metal foam, perforated plate, diamond-shaped structure) showed noise reductions up to 12 dB at St = 0.12 for Ma = 0.5. Far-field and beamforming analyses revealed that permeable materials shift the dominant acoustic source away from the trailing edge, mitigating scattering-induced noise. The results demonstrated that even low-permeability structures could significantly reduce noise by altering the dominant radiation mechanisms, thus advancing aeroacoustic mitigation strategies.

Chen et al. (2023) [8] investigated the effects of wall proximity on vortex-induced vibrations (VIV) of an elastically mounted circular cylinder at Reynolds numbers ranging from 1.77×10^3 to 1.24×10^4. The study varied the gap-to-diameter ratio $e^* = e/D$ between 0.1 and 1.6 to examine its influence on vibration amplitude, vortex shedding frequency, and flow structure. Using laser vibrometry, hot-wire anemometry, and particle image velocimetry, the authors found that decreasing e^* increases added mass and significantly reduces vibration amplitude and VIV range, while enhancing the quality factor. Notably, when $e^* < 0.6$, flow structures displayed increased asymmetry and higher time-mean lift forces, indicating intensified wall-cylinder interactions. These findings advance the understanding of wall interference effects in fluid–structure interactions.

Rokicki et al. (2023) [9] introduced a novel diagnostic approach for steam turbine blades using the Metal Magnetic Memory (MMM) method to identify operational modal frequencies and shapes. The method measures residual magnetic field (RMF) distributions, which correlate with stress wave patterns resulting from blade vibrations. By analyzing these RMF patterns and comparing them with finite element method (FEM) simulations, the study confirms that operational modeshapes closely align with the blade's 10th natural frequency (~1014 Hz). This technique enables non-invasive, real-time monitoring of structural dynamics and stress concentration zones, offering valuable insight into the long-term health of turbine blades.

Ren et al. (2024) [10] presented a comprehensive review of stiffness enhancement strategies for thin-walled aircraft structures, which are increasingly vulnerable to vibration and thermal buckling under extreme service conditions. The review categorizes passive method, such as stiffening via laminated plates, and active methods involving smart materials with adaptive properties. The authors critically analyzed technical challenges associated with implementation, including integration, material compatibility, and structural complexity. The paper concludes by outlining the future role of multifunctional smart materials in next-generation aerospace systems and emphasizes the importance of balancing weight reduction with mechanical resilience.

Chu et al. (2024) [11] reviewed the fundamentals and industrial applications of vibration analysis (VA) in predictive maintenance, emphasizing its diagnostic capabilities for early fault detection across a wide range of equipment and sectors. The review highlights VA's effectiveness in minimizing downtime and repair costs and discusses its growing use in the petroleum industry, particularly in Electric Submersible Pumps (ESPs), which are challenging to monitor due to their downhole location. Studies utilizing principal component analysis (PCA) and vibration signal processing are evaluated, with findings showing potential for predictive diagnostics. The paper advocates for expanded research into VA applications in petroleum production systems to enhance system reliability and efficiency.

Fahmi et al. (2022) [12] offered a critical review of mechanical failure mechanisms that induce vibration in gas turbines used in combined cycle power plants (CCPPs). The study identifies key vibration-inducing phenomena such as rotor-stator rubbing, unbalance, mis-

alignment, critical speed issues, and electromagnetic faults (e.g., shorted turns). The review also discusses widely used diagnostic technologies, such as proximity probes, laser Doppler vibrometry, eddy current sensors, and accelerometers, that facilitate real-time monitoring and maintenance scheduling. The authors emphasize the economic and operational value of high-accuracy vibration detection for failure prevention in CCPP turbines.

Xie et al. (2022) [13] proposed a blade damage monitoring method based on the frequency-domain statistical indices of shaft's random vibration signals. A dynamic continuum model of a blade-disk-shaft system incorporating bending-torsional coupling was developed and experimentally validated. The methodology filters out forced harmonic vibrations and isolates the random vibration component, from which mean frequency and bandwidth indices in the resonance band are extracted as damage indicators. The approach demonstrated high sensitivity to structural faults in experimental setups, providing a practical and efficient tool for in-situ health monitoring of rotating blades using easily measurable shaft vibrations.

As indicated by Kumar and Tiwari [14] in their review paper, non-contact vibration measurement techniques are significantly applicable in aircraft engine diagnostics. Another example of monitoring the condition of the engineering system by vibration analysis is the paper of Djaidir et al. [15], in which faults were detected in a gas turbine rotor using vibration analysis.

Diagnostics by application of laser vibrometry is the future direction addressing the most important challenges in this area; although it has been known for years [16,17], it has not become a common technique as a diagnostics tool. As shown in the literature, the use of Fourier transform in the vibration analysis of aircraft engines gives promising results, as seen in Jia et al. [18]. Such diagnostics of advanced vibration analysis techniques supported by machine learning algorithms is the future for jet engine diagnostics, particularly in identifying faults, as shown recently by Tama et al. [19].

Modern aircraft operated by air forces, despite functioning within their specified technical parameters, increasingly require advanced diagnostic procedures. The current body of literature presents numerous studies dedicated to the development and application of innovative measurement and analysis techniques aimed at detecting potential damage in engine modules and their components. For example, Prokopowicz [20] has conducted extensive research on the implementation of such methods to support faster module replacements, thereby enhancing the operational availability of propulsion systems.

A notable contribution is Guminiak's work [21], which demonstrated the effectiveness of discrete wavelet transform in damage detection, particularly in structural components such as plates. This approach enables the accurate identification and localization of defects. Similarly, Nowakowski and Komorski [22] developed self-diagnostic systems utilizing high-frequency vibration measurements, enabling early-stage fault detection and improving the overall reliability of engine components.

Further advancements include the use of neural network algorithms, as demonstrated by Tabaszewski et al. [23], where vibration signals were used to assess engine valve clearance. This application highlights the potential of artificial intelligence in diagnosing complex engine parameters with high precision. Importantly, novel diagnostic approaches are not limited to vibration analysis alone. Acoustic diagnostics have also shown promise, as evidenced by the research conducted by Nowakowski et al. [24]. Even minor enhancements to existing diagnostic procedures can yield substantial practical benefits. For instance, Grądzki et al. [25] introduced a subtle modification to the diagnostic method for rotor blades, enabling the early detection of critical failures.

Innovative measurement techniques supported by advanced signal processing, numerical simulations, and machine learning can significantly enhance both the accuracy and

depth of diagnostic insights [26–29]. Numerous studies have confirmed the value of such approaches in testing and monitoring complex machinery and processes [30].

Laser-based measurement techniques also play a pivotal role in modern diagnostics. Tang et al. [31], for example, investigated turbine blade wear using a laser sensor to track blade vibrations. In addition, spectral analysis of vibration data can be employed to assess wear characteristics and predict the onset of damage. By analyzing vibration velocity and frequency patterns in relation to known operational data for a given engine population, it is possible to isolate the faulty component and determine necessary corrective actions.

In this paper, we present a vibration analysis of a turbojet engine to identify the root causes of abnormal vibration behavior. This study was divided into two phases: the first involving a turbojet engine exhibiting increased vibration amplitudes, and the second utilizing an engine operating within normal vibration limits as a reference. Vibration data were collected from the compressor and turbine housing, and power spectral analysis was applied to evaluate the condition of the rotating machinery. The resulting parameters were used to diagnose the condition of the engine rotor system and propose targeted mitigation strategies.

The analysis revealed that excessive vibration was primarily caused by rotor mass imbalance, attributed to wear of the main support bearings. Additional issues included misalignment of the main rotor shaft and uneven radial stiffness in the turbine section. Furthermore, potential dynamic and static friction anomalies in the turbine rotor seal were identified. These findings confirmed the validity of the proposed vibration analysis procedure for routine servicing on engine test benches.

The insights gained from this study lay the foundation for integrating artificial intelligence in fault analysis using learning algorithms, particularly those operating in the time-frequency domain. Comparable vibration testing and diagnostic methodologies are already employed by leading engine manufacturers, such as Rolls-Royce (e.g., pass-off testing of the Pegasus engine) and Pratt & Whitney. However, the Polish Air Force lacks access to proprietary diagnostic databases provided by these manufacturers. Consequently, it is essential to develop and maintain a national diagnostic dataset for the F100-PW-229 engines currently in use [32].

The method proposed in this study is analogous to techniques applied in internal combustion engine diagnostics and consists of three key stages:

- Signal preprocessing using decomposition algorithms,
- Multi-domain parameter estimation (time and frequency),
- Supervised feature selection via the Relief-F algorithm.

Among many feature selection techniques, Relief-F is considered particularly effective due to its high efficiency and flexibility in handling diverse data types [33,34]. The proposed analysis begins with decomposing the vibration velocity spectrum into constituent signals, characterized in both time and frequency domains. These results are then benchmarked against findings in the literature for comparable jet engine systems.

2. Materials and Methods

The present research proposes a vibroacoustic analysis procedure for the Pratt & Whitney F100-PW-229 engine (East Hartford, CT, USA) during tests on an engine test bench using non-contact laser measurement systems. As reviewed in the scientific literature, studies addressing this or similar topics are scarce. The solution presented here significantly reduces measurement time, does not require the installation of additional instrumentation, and allows vibration data collection from any area of the engine's external structure and attached units. Measurements can be taken from distances up to thirty meters, and the process is safe for the operator. Initial measurements using this method serve to develop a

vibration map of the F100-PW-229 engine, which forms the basis for introducing additional maintenance procedures.

Therefore, we present a new approach for measuring and analyzing vibrations in aircraft engines based on laser systems. The measurements were performed using POLYTEC VibroGo VGO-200 laser sensors (Waldbronn, Germany). Figure 1 shows the Pratt & Whitney F100-PW-229 engine, which powers the F-16 aircraft and is the focus of this research. Two engines were compared: one exhibiting increased vibration amplitude during operation and the other displaying a low vibration footprint. Both engines were tested on an engine test bench under the same environmental conditions.

Figure 1. Measurement station of POLYTEC VibroGo VGO-200 device.

In this study, a laser accelerometer was used to measure displacement velocity in order to assess the vibration of the bearings in the engine supports. The measurement system consisted of the VibroGo VGO-200 vibrometer and the SIGVIEW v5.3.2 data analysis software. Vibrations were recorded in a plane perpendicular to the engine axis during testing. The vibrometer enabled measurements in mutually perpendicular planes by analyzing the phase of the laser beam. However, a single laser beam allowed measurement at only one point at a time. The direction of the vibration measurements was chosen based on the trajectory of the shaft pivot within the support bearings (see Figure 2). This trajectory was affected by motor damage or wear, as well as by the bearings' uneven directional sensitivity [20].

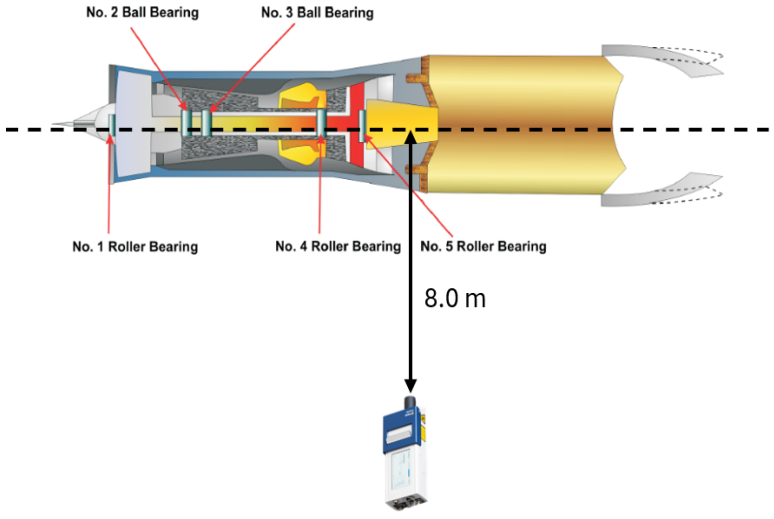

Figure 2. Layout of the individual supports of the P&W F100-PW-229 engine: fan inlet bearing, forward section and gearbox bearing, and turbine bearing and fan drive turbine bearing path of the shaft pivot in support bearings [32].

The Pratt & Whitney F100-PW-229 is a dual-flow jet engine with an annular combustion chamber and a mixed-flow booster. The engine incorporates variable blades at the inlets of both compressors and a variable exhaust nozzle. The rotating sections are supported by five main bearings (Figure 2). In addition, the engine is constructed from five modules (Figure 3), which facilitates maintenance and repair work. The first module is a three-stage fan that supplies compressed air to the intermediate housing, where the airflow is divided between the main engine ducting and the external ducts. The core engine module produces high-pressure hot gases that rotate the rear compressor and turbine; the remaining energy goes to the exhaust nozzle module. This core engine module houses a bevel gearbox that drives the accessory gearbox and the drive shaft to operate the airframe aggregates. A compressor provides a suitable coupling point between the fan rotor and the turbine shaft driving the fan. The turbine assembly is a ten-stage compression design based on axial flow, with a compression ratio of 8:1. The compressor stator contains variable fourth- and fifth-stage blades, mechanically connected to the blade assembly. The diffuser housing section consists of a diffuser housing, 24 fuel nozzles, a combustion chamber (annular design), a first-stage nozzle guide vane assembly, and a no. 4 bearing. This roller bearing on the compressor drive shaft maintains radial alignment between the compressor tail rotor and stator housing [35]. Roller bearing no. 5, located inside the rear end of the fan drive turbine shaft, maintains radial alignment between the fan drive turbine and the turbine housing.

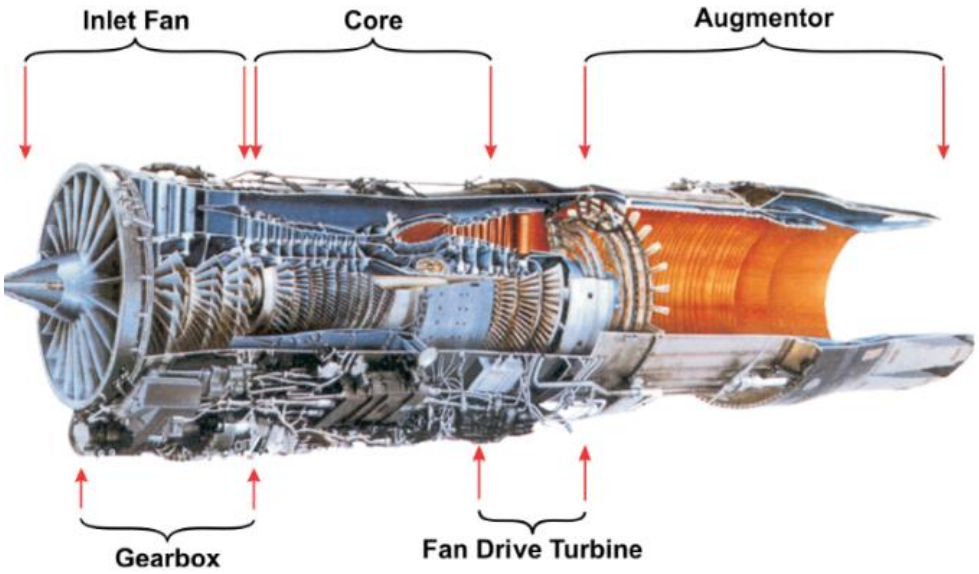

Figure 3. Individual modules of the P&W F100-PW-229 engine [32].

During engine operation, the gearbox module receives torque from the compressor via gears and transmits it to the accessory drive gearbox via the shaft (aircraft power take-off shaft). At engine start-up, torque is transmitted in the reverse direction.

In the presented study, the engine was mounted on the airframe using a four-point mounting system that aligns the engine with the inlet fairings and the rear of the fuselage precisely. The mounts were designed to support the engine without carrying airframe loads while protecting from engine temperature rise during operation. During the engine test bench testing, the engine was mounted on a test stand in the form of an engine trolley, similar to the one shown in Figure 4.

Figure 4. The F100-PW-229 engine on the test bench.

3. Results

Vibration data obtained from measurements with the POLYTEC VibroGo VGO-200 device, in the form of the velocity of change of vibration amplitude, is subjected to Fourier analysis. The analysis is performed using the SIGVIEW v. 5.0.0.0 software from SignalLab.

The relation describing the transition to the frequency domain for a discrete signal is the discrete Fourier transform:

$$X(k) = \frac{1}{N}\sum_{n=0}^{N-1} X(n) exp\left(-i\frac{2\pi kn}{N}\right) \tag{1}$$

The inverse transform takes the form:

$$X(n) = \sum_{k=0}^{N-1} X(k) exp\left(-i\frac{2\pi kn}{N}\right) \tag{2}$$

where:

N—the number of time samples used in the analysis;
n—the sequence number of the time sample;
k—the sequence number of the frequency sample.

Equations (1) and (2) show that, for N frequency components, N^2 complex multiplications are performed, which has a high computational cost. Therefore, the fast Fourier transform (FFT) algorithm is used in practice [36] and also was used in this analysis.

To calculate the FFT transform of a vibration signal of length Q, the recorded waveform in the time domain is first multiplied by a rectangular function $w_{pros}(t)$ called the rectangular window:

$$w_{pros}(t) = \begin{cases} 1 & for\ t \in < -\frac{Q}{2}, +\frac{Q}{2} > \\ 0 & for\ t \notin < -\frac{Q}{2}, +\frac{Q}{2} > \end{cases} \tag{3}$$

where:

t—time of the signal,
Q—length of signal.

The Fourier transform of this rectangular window is given by:

$$W_{pros} = \int_{-\infty}^{+\infty} w_{pros}(t) exp(-i2\pi ft)dt = \int_{-\frac{Q}{2}}^{+\frac{Q}{2}} exp(-i2\pi ft)dt = \frac{1}{i2\pi f}[exp(-i2\pi ft)]_{-\frac{Q}{2}}^{+\frac{Q}{2}} = Q\frac{sin(\pi fQ)}{(\pi fQ)} \tag{4}$$

The FFT algorithm requires a signal length Q such that the number of samples is an integer power of two. Taking the number of obtained signal samples as N raised to a power of two and applying the "zero-padding" procedure (complementing the signal with such a number of zeros that the signal length condition is fulfilled corresponding to the number of samples as a power of two) if necessary, to increase the signal length to the required value, the FFT of an appropriately transformed Hamming window, given in the time domain by the formula [36]

$$x(n) = 1 - 2\alpha - 2\alpha cos\left(\frac{2\pi n}{N}\right) dla\ n = 0,\ 1,\ 2,\ \ldots,\ N-1 \tag{5}$$

is applied, with the resolution loss factor:

$$\eta_\alpha = \frac{1 - 4\alpha + 6\alpha^2}{(1-2\alpha)^2} \tag{6}$$

The case of $\alpha = 0$ indicates an ordinary rectangular window, while $\alpha = 0.25$ implies the cosine Hamming window used in the analysis [36].

Without losing the required resolution of the signal analysis, the window makes extracting the characteristic components of the spectrum possible, despite the scattering of part of the signal power in the side lobes.

To analyze the vibration signal of the F100-PW-229 motor, $N = 2.5 \times 10^4$ samples were recorded for each measurement point. Fourier analysis was chosen because it is simple and efficient to calculate and can obtain a real-time spectrum. With this analysis method, a real-time signal composed of N samples yields a spectrum represented by $N/2$ samples, and the amount of information is reduced by half. The number of parameters describing the spectrum depends on the length of the signal in the time domain, making classification procedures difficult even for statistical and artificial intelligence-based methods, such as genetic algorithms.

In principle, the vibration velocity (integrated acceleration over time) strongly correlates with the energy transferred by vibrational motion. However, vibration acceleration can reveal some phenomena that are not apparent in the velocity signal. Both quantities are useful in a holistic approach to vibroacoustic analysis. The present study focuses on the analysis of the vibration velocity signal of the F100-PW-229 motor, allowing changes in vibration amplitude to be isolated at characteristic frequencies. In this analysis, the range of the useful vibration spectrum of the motor is assumed to range from 1 to 250 kHz [35].

During the tests, vibration data were recorded for two Pratt & Whitney F100-PW-229 engines. The first showed no symptoms of increased vibration, while the second caused vibrations in the airframe on which it was installed. Both engines were tested on the engine test bench in a Polish Air Force (PLAF) airbase laboratory/workshop. To determine potential damage to engine components, such as the bearings (supports) of the compressor (Figure 5, measurement point 1) and turbine shafts (Figure 5, measurement point 2), rotor blade rims of the individual compressor and turbine stages (Figure 5, measurement point 3), combustion chambers with spark gaps, and gearbox of the accessory drive box (Figure 5, measurement point 4), the most critical measurement areas were selected, as shown in Figure 5. Vibrations were measured at these points by illuminating them with the laser beam of the VibroGo VGO-200 device at a distance of eight meters in an enclosed engine test bench room. The laser beam measured vibrations in a plane perpendicular to the laser beam.

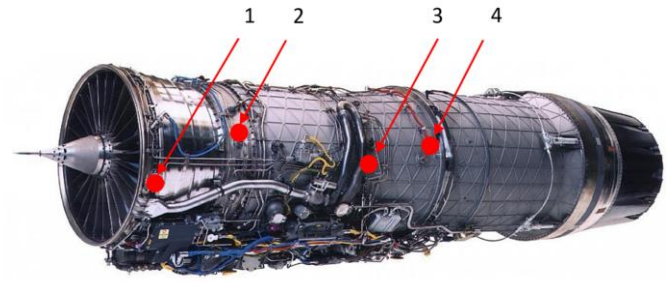

(**a**)

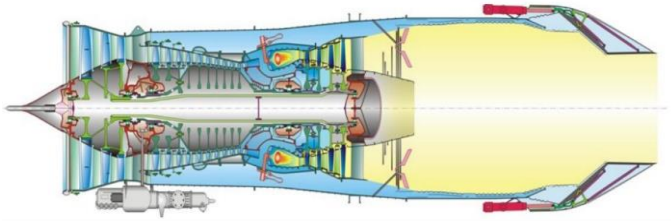

(**b**)

Figure 5. Location of measurement points illuminated by the laser beam of the VibroGo VGO-200: (**a**) exterior view of the Pratt & Whitney F100-PW-229 [graphic by Pratt & Whitney] (Source: http://www.f-16.net/, accessed on 1 November 2024) and (**b**) cross-section [37].

The recorded signal was then analyzed. First, the components of the spectrum characteristic of the engine design elements selected were determined analytically. Figure 6 shows an atypical jet engine vibration spectrum, expressed on the decibel scale [38].

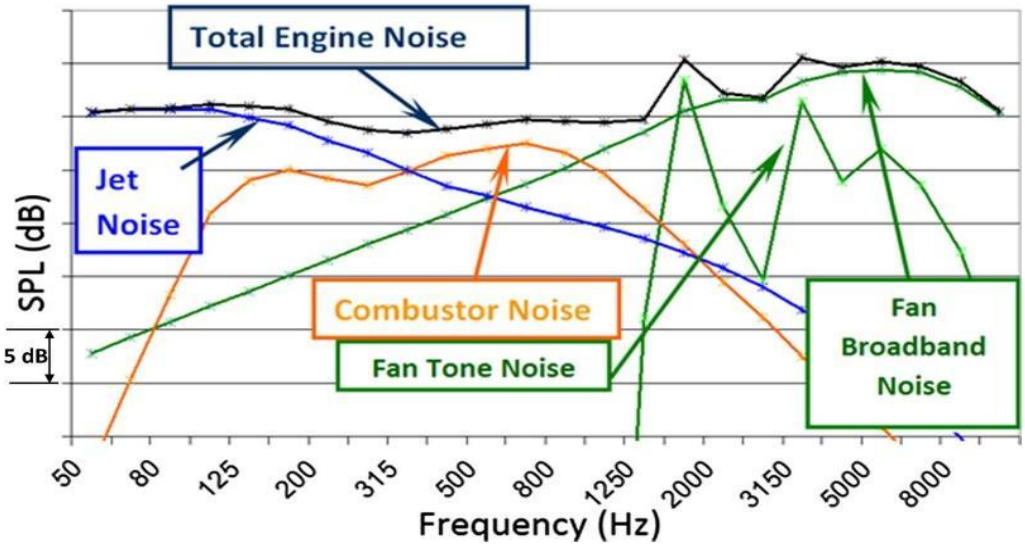

Figure 6. Characteristic noise spectrum of a turbojet engine on approach (source: SAFRAN Snecma, http://www.safran-group.com/, accessed on 1 November 2024).

The characteristic spectrum ranges for the fan are shown in green in Figure 6. The vibration spectrum for the combustion chamber is orange, and the spectrum characteristic of the various phenomena occurring in the chamber is shown in black. Analytical calculations determine the characteristic frequency ranges present in the spectrum (mainly for the engine shaft, roller bearings, and gears). For the compressor and turbine blade rims, on the other hand, the results were cross-referenced with those available in the literature.

The characteristic components related to shaft speed for low-pressure compressor speeds [33,39] are

$$f_{OSNC} = \frac{n_1}{60} = \frac{4100\ [\text{rpm}]}{60} = 68\ [\text{Hz}] \tag{7}$$

$$f_{OSWC} = \frac{n_2}{60} = \frac{10,100\ [\text{rpm}]}{60} = 168\ [\text{Hz}] \tag{8}$$

where

f_{OSNC}—low-pressure compressor shaft frequency;
f_{OSWC}—high-pressure compressor shaft frequency;
n_1, n_2—the motor shaft speeds (rpm) for the idles speeds of 4100 and 10,100 rpm, respectively.

Subsequent spectrum components identical to the potential bearing properties of engine supports 1–5 are calculated by the following.

- The frequency corresponding to the bearing cage is

$$f_K = \frac{1}{2} \cdot f_r \left(1 - \frac{BD}{PD} cos\beta\right) \tag{9}$$

where:

BD—diameter of the rolling element (m);
PD—pitch diameter of the bearing;
β—contact angle between the rolling element and raceway (for an ordinary ball bearing, $\beta = 0$);
f_r—frequency related to the motor shaft speed (low-pressure compressor f_r = 68 Hz; low-pressure compressor f_r = 168 Hz).

- The frequency corresponding to the failure of the rolling element is

$$f_{ET} = f_r \frac{PD}{BD} \left[1 - \left(\frac{BD}{PD} cos\beta\right)^2\right] \tag{10}$$

- The frequency corresponding to the failure of the inner raceway is:

$$f_{BW} = f_r \frac{n_k}{2} \left[1 \pm \left(\frac{BD}{PD} cos\beta\right)\right] \tag{11}$$

where

n_k—the number of rolling elements in the bearing and the $\pm$ signs indicate the inner and outer raceway, respectively.

When calculating the vibration frequency of turbine and compressor rims, we use the relationship

$$f_w = z \frac{n}{60} \tag{12}$$

where

f_w—vibration frequency for individual compressor or turbine rims (Hz);
n—motor shaft speed (rpm);
z—the number of blades on individual rims.

The value of the characteristic frequencies of the gears are determined from the relationship

$$f_{PZSNAS} = i \frac{n}{60} \tag{13}$$

where

n—motor shaft speed.

$$i = \frac{z_1 - z_2}{z_1} \tag{14}$$

where:

i—geometric gear ratio determined by the ratio of the number of teeth on the individual gear wheels z_1 and z_2.

The quantities of rolling elements in the bearings are shown in Table 1.

Table 1. Quantities of rolling elements in the bearings.

Support No.	Bearing Type	Number of Rolling Elements	Type of Rolling Element
1	Rolling	20	Roller
2	Ball	20	Ball
3	Ball	18	Ball
4	Rolling	32	Roller
5	Rolling	22	Roller

The data in Table 1 were obtained from the engine technical documentation, actual measurements of spare parts remaining in the equipment of the Engine Maintenance Workshop of the Airbase Technical Squadron, and the FEDLOG database [40]. In addition, the characteristic frequencies of the spectrum, calculated using the relationships (7–14), are listed in [40], along with the technical parameters of the engine bearings.

During the tests, the amplitude of the characteristic frequencies of the spectrum for the compressor shaft speed increased at both speed ranges of the motor showing vibration symptoms, f_{OSNC} = 68 Hz and f_{OSWC} = 168 Hz (from (7) and (8), respectively). This may indicate backlash or unbalance of the low-pressure compressor rotor shaft. Characteristic frequencies that are indicative of this type of failure are an increase in the value of the amplitude of 1 f_{OSNC} = 68 Hz, 2 f_{OSNC} = 136 Hz, and 3 f_{OSNC} = 205 Hz (Figures 7–9). What is more, there is an increase in the value of the amplitude of these frequencies for the damaged engine but not for the third harmonic. However, a slight shift in the spectrum for both motors is evident from 2 f_{OSNC} = 136 Hz to 2 f_{OSNC} = 117 Hz, which could be caused by the frequency-domain signal process. All indicated harmonics are present in the vibration spectra of both motors, but the amplitude is significantly higher for the potentially faulty motor. The percentage amplitudes of the individual harmonics are determined by performing additional tests on this type of motor.

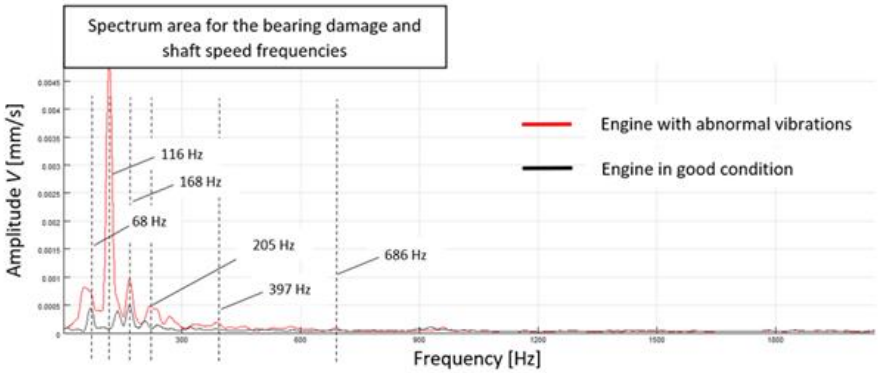

Figure 7. Vibration analysis point no. 1 for the relevant frequency ranges of spectrum frequencies up to 2 kHz.

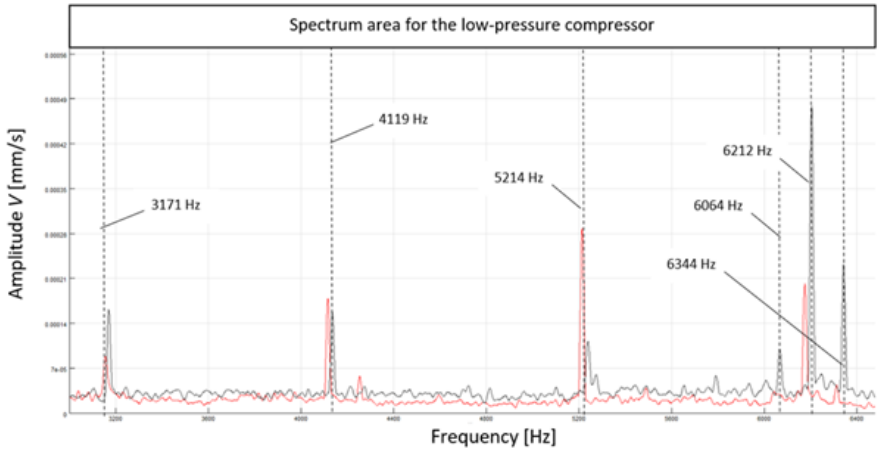

Figure 8. Vibration analysis point no. 1 for the relevant frequency ranges of spectrum frequencies 2–7 kHz.

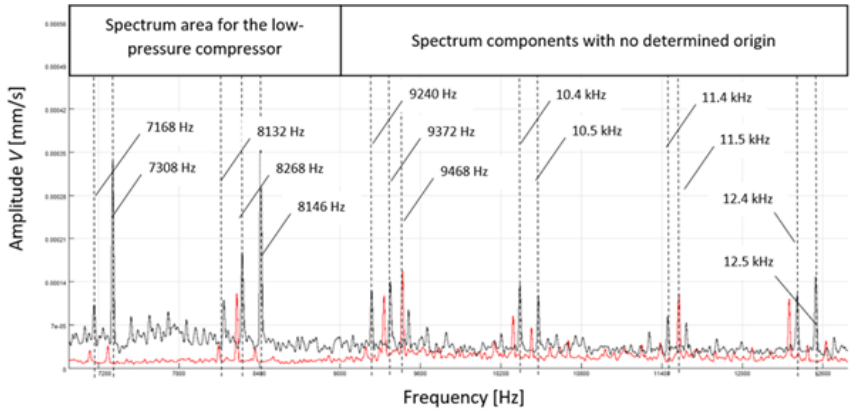

Figure 9. Vibration analysis point no. 1 for the relevant frequency ranges of spectrum frequencies 6–13 kHz.

The remainder of the analysis focuses on the engine's internal structural elements, such as the bearings of the individual supports. Frequencies determined for the various types of damage are listed in Tables 2–5 and defined below:

- f_K—damage to the bearing cage of the first support;
- f_{ET}—damage to the rolling element;
- f_{BW}—damage to the inner raceway;
- f_{BZ}—damage to the outer raceway;
- f_{PBW}—undulations of the inner raceway;
- f_{PBZ}—undulations of the outer raceway;
- f_{SNCP}—frequency of aeromechanical vibrations of the rotor coming from the blades on the rims of a low-pressure compressor for individual stages;
- f_{SWCP}—frequency of aeromechanical vibrations of the rotor coming from the blades on the rims of a high-pressure compressor for particular stages;
- f_{AKSWC}—frequency of aeromechanical vibrations of the rotor coming from the steering vanes of the high-pressure compressor for particular stages;
- f_{PZSNAS}—frequency corresponding to gearbox failure of the motor aggregate drive box.

Table 2. Components of the engine vibration spectrum related to the internal structural elements tested in selected engine regions—first measurement point.

Tested Element	Spectral Component [Hz]	
	Calculated	**Measured**
Bearing no. 1	f_K = 33 f_{ET} = 398	– 392
	f_{BW} = 308 f_{BZ} = 292	206–292
	f_{PBW} = 665 f_{PBZ} = 3965	684 –
Vibrations of the rotor coming from the blades on the rims of a low-pressure compressor for individual stages	f_{SNCP} (stage 1) = 3553 f_{SNCP} (stage 2) = 3963 f_{SNCP} (stage 3) = 4783	3171 4119 5214

Table 3. Components of the engine vibration spectrum associated with the internal structural elements studied in selected engine regions—second measurement point.

Tested Element	Spectral Component [Hz]	
	Calculated	**Measured**
Bearing no. 2	f_K = 30 f_{ET} = 89	– 87
	f_{BW} = 335 f_{BZ} = 265 f_{PBW} = 604 f_{PBZ} = 832	336 264–295 – 830
Bearing no. 3	f_K = 34 f_{ET} = 130 f_{BW} = 328 f_{BZ} = 332 f_{PBW} = 688 f_{PBZ} = 1303	– 138 335 335 677–719 –
Vibrations of the rotor coming from the blades on the rims of a high-pressure compressor for particular stages	f_{SWCP} (stage 4) = 4783	–
	f_{SWCP} (stage 5) = 5193	5213
	f_{SWCP} (stage 6) = 6013	6076
	f_{SWCP} (stage 7) = 6650	6619
	f_{SWCP} (stage 8) = 6287	6195
	f_{SWCP} (stage 9) = 6833	6885
	f_{SWCP} (stage 10) = 7380	7283
	f_{SWCP} (stage 11) = 8200	8251
	f_{SWCP} (stage 12) = 8200	8251
	f_{SWCP} (stage 13) = 8337	8383
Vibrations of the rotor coming from the steering vanes of the high-pressure compressor for particular stages	f_{AKSWC} (stage 4) = 70	66
	f_{AKSWC} (stage 5) = 76	–
	f_{AKSWC} (stage 6) = 88	87
	f_{AKSWC} (stage 7) = 96	–
	f_{AKSWC} (stage 8) = 92	–
	f_{AKSWC} (stage 9) = 100	–
	f_{AKSWC} (stage 10) = 108	–
	f_{AKSWC} (stage 11) = 120	118
	f_{AKSWC} (stage 12) = 120	118
	f_{AKSWC} (stage 13) = 122	–
Accessory drive box gearbox	f_{PZSNAS} = 2727	2880

Table 4. Components of the engine vibration spectrum related to the internal structural elements studied in selected engine regions—third measurement point.

Tested Element	Spectral Component [Hz]	
	Calculated	**Measured**
Bearing no. 4	f_K = 34	–
	f_{ET} = 222	219–237
	f_{BW} = 328	–
	f_{BZ} = 331	–
	f_{PBW} = 686	682
	f_{PBZ} = 2226	2224

Table 5. Components of the engine vibration spectrum associated with the internal structural elements studied in selected engine regions—fourth measurement point.

Tested Element	Spectral Component [Hz]	
	Calculated	**Measured**
Bearing no. 5	f_K = 34	44
	f_{ET} = 878	–
	f_{BW} = 330	–
	f_{BZ} = 330	–
	f_{PBW} = 684	698
	f_{PBZ} = 8779	–

Starting from the first roller bearing, characteristic spectral components f_{ET} = 392 Hz, f_{BW} and f_{BZ} in the spectral range 206–292 Hz, and f_{PBW} = 684 Hz were observed, which could be indicative of damage to the rolling elements and the inner and outer races of the bearing.

4. Discussion

The low-pressure compressor (SNC) showed an increase in vibration for the faulty motor relative to the reference motor towards the higher stages. In conjunction with the significant increase in vibration amplitude for the first support bearing, we conclude that the vibration propagated from the bearing towards the blade rims.

Measuring only the radial vibration of the blades of individual SNC rims to the rotating components does not allow us to unambiguously determine the damage at the attachment points of the blades or the entire rims. For this purpose, additional tests are necessary with the same device, performed axially and tangentially to the rotating components.

In the case of the second bearing, the characteristic spectrum components associated with its damage, confirmed by calculations, occurred at the frequencies f_{ET} = 87 Hz, f_{BW} = 336 Hz, f_{BZ} = 265–292 Hz and f_{PBZ} = 830 Hz (Figures 10 and 11). These frequency occurrences suggest damage to the rolling elements and abnormalities in the structure of the inner and outer raceways of this bearing.

The next component subjected to vibroacoustic tests is the gearbox drive gear, for which a characteristic frequency f_{PZSNAS} of 2727 Hz was calculated according to (13) and (14). The closest frequency of the spectrum that can correspond to the gear is f_{PZSNAS} = 2880 Hz. Exceeding the amplitude of this component concerning the corresponding partiality of the reference motor indicates potential backlash in the gearbox (Figure 8).

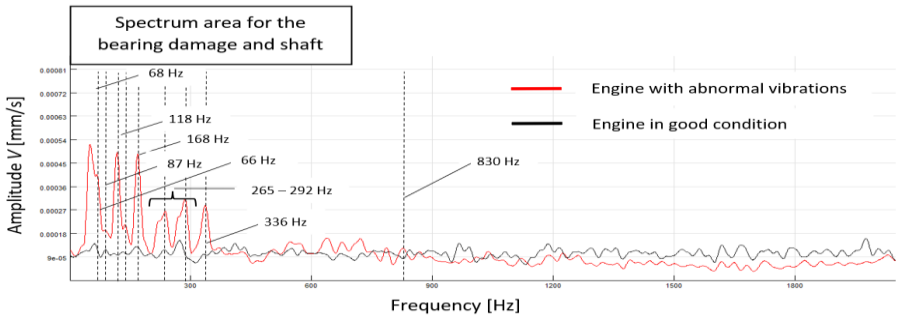

Figure 10. Vibration analysis point no. 2 (bearings no. 2 and 3) for the relevant frequency ranges up to 2 kHz.

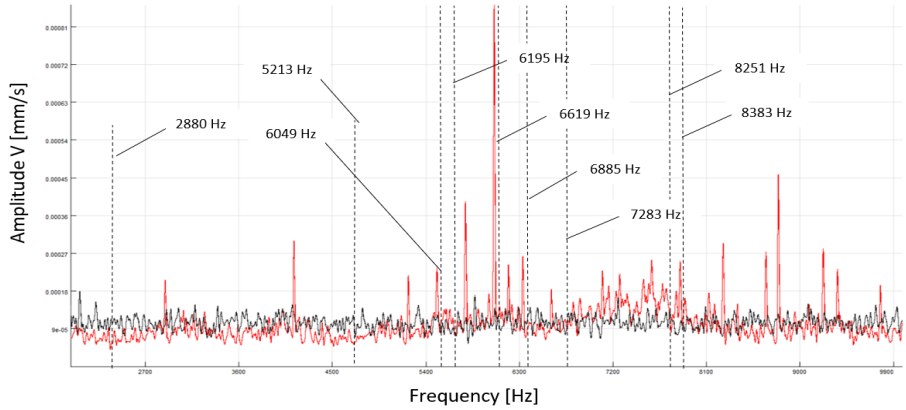

Figure 11. Vibration analysis point no. 2 (bearings no. 2 and 3) for the relevant frequency range 2–10 kHz.

In the spectral range of 5–10 kHz, several components exhibited increased amplitudes relative to the reference engine spectrum similar to the rotor aeromechanical vibration frequency from the high-pressure compressor blades f_{SWCP} (Table 1). This included components specific to the blade rims of the individual stages. All components of the spectrum for the compressor rims showed increased amplitude compared to the reference engine. Similarly to the SNC, the high compressor(SWC) showed an increase in vibration associated with significantly higher vibration amplitudes for the second and third support bearings. The test results indicate that the vibrations propagated from the bearings toward the blade rims. Again, measuring only the radial vibrations of the blades of individual SWC rims to the rotating components does not identify damage at the blade mounting points or the entire rims. Therefore, we must carry out tests with the same device axially and tangentially to the rotating components.

To determine the vibration spectrum of the low- and high-pressure turbines, we relate the test results to those presented by Maynard and Trethewey [41,42]. The results of the torsional vibration of the jet engine turbine blades for shaft speeds of 9000 and 9450 rpm are shown in Figure 12.

Figure 12 shows that the range of characteristic frequencies from the high-pressure turbine components is between 2.2 and 5.6 kHz. Compared with the test results of the F100-PW-229 engine, the amplitude of the vibration components of the spectrum of this engine increased, corresponding to the blades of the high-pressure turbine for measurement points 3 and 4 (Figure 5). Additional tests on individual rims are necessary to determine the components for individual blades.

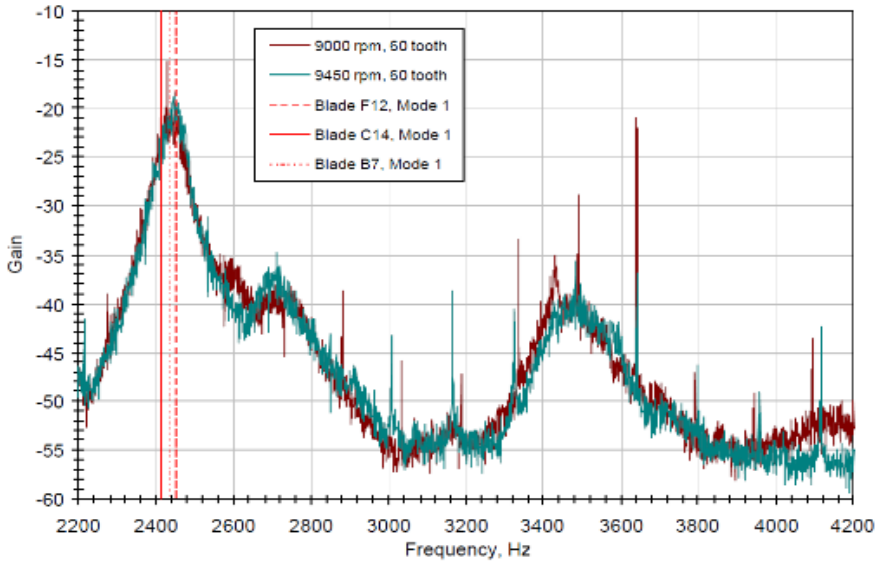

Figure 12. Torsional spectrum of a high-pressure turbine of a typical jet engine (Source: [41]).

The torsional vibration of rim blades in rotating machinery is related to the oscillatory and angular motion of the rotating shaft on which they are mounted. This motion has the effect of loosening the blade bed, causing deformation and fatigue defects [43]. Torsional vibrations can also be seen as cyclical changes in shaft speed [44]. The engine shaft is not indifferent to changes in the blade rims, as any changes in the blade structure can cause it to fracture [45]. Research by C. H. Yang and S. C. Huang [46,47] showed a correlation between blade bending, twisting, and vibration and shaft damage propagation based on a theoretical model of the shaft–disc kinematic joint. The characteristic vibration of compressor blades can be extracted from the vibration spectrum of the shaft on which their rims are mounted. Studies of the relationship between blade bending and shaft damage were conducted by Huang and Ho [48] and Al-Bedoor [49]. Their research showed the occurrences of components in the vibration spectrum of the engine shaft that are characteristic of blade rim vibrations for both the compressor and the turbine, which could be used to assess their technical condition (Figures 10–18).

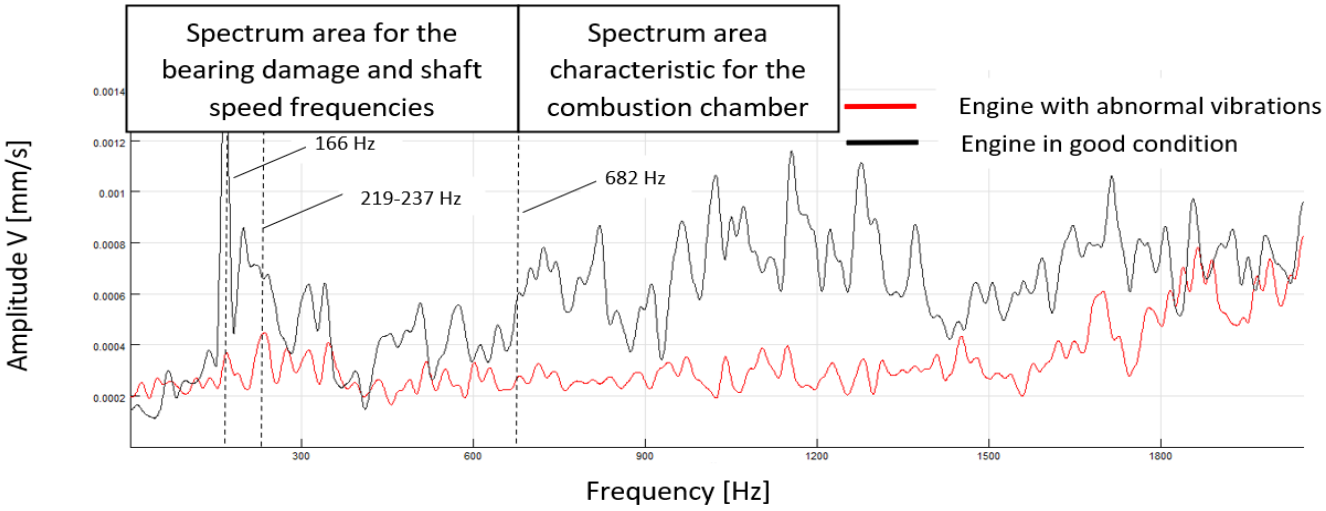

Figure 13. Vibration analysis point no. 3 (bearing no. 4), for the relevant frequency ranges up to 2 kHz.

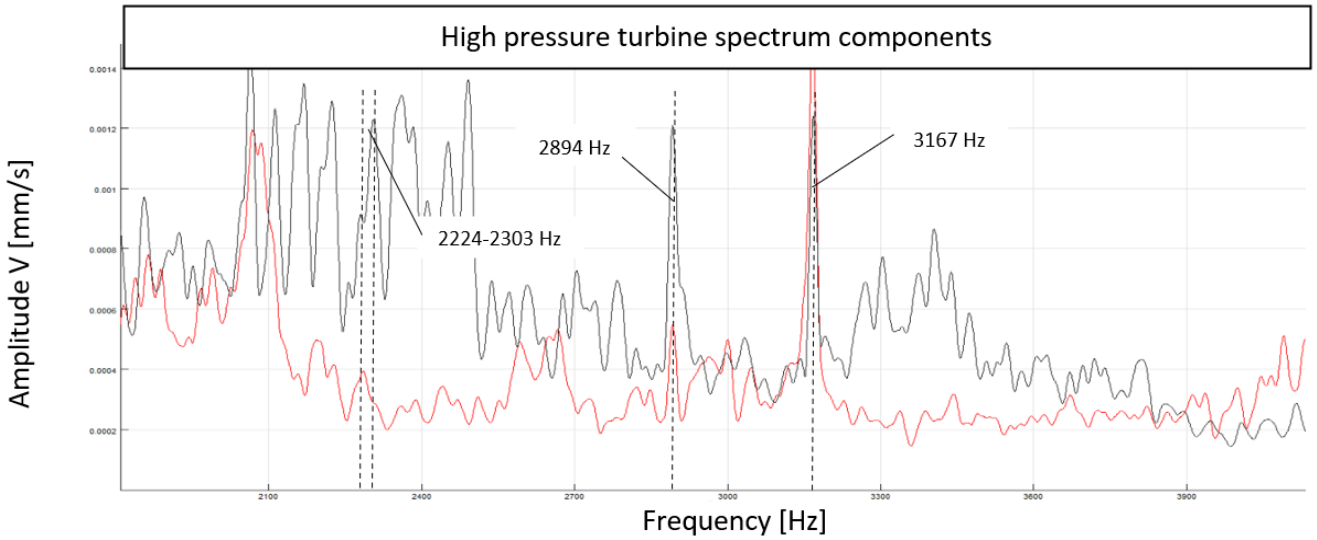

Figure 14. Vibration analysis point no. 3 (bearing no. 4), for the relevant frequency ranges up to 2–4 kHz.

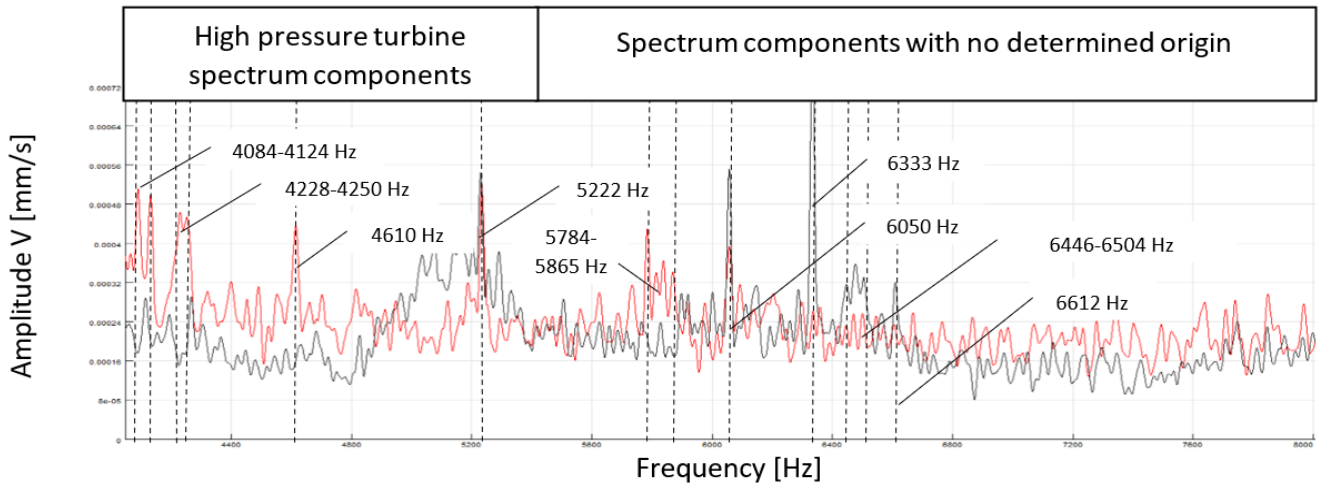

Figure 15. Vibration analysis point no. 3 (bearing no. 4), for the relevant frequency ranges up to 4–8 kHz.

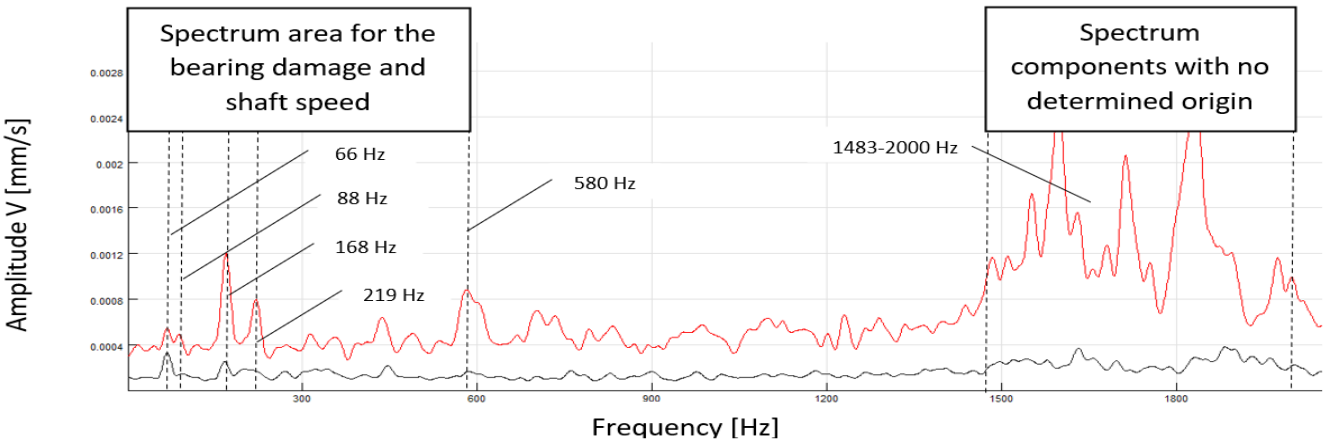

Figure 16. Vibration analysis point no. 4 (bearing no. 5) for the relevant frequency ranges up to 2 kHz.

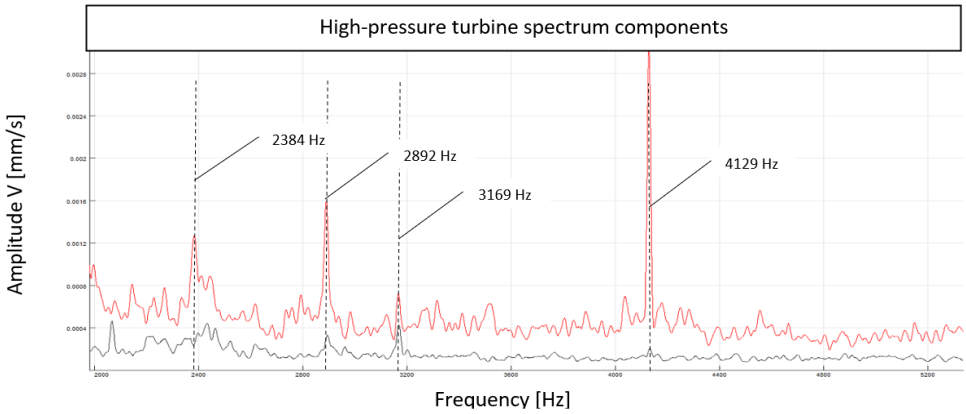

Figure 17. Vibration analysis point no. 4 (bearing no. 5) for the relevant frequency ranges 2–6 kHz.

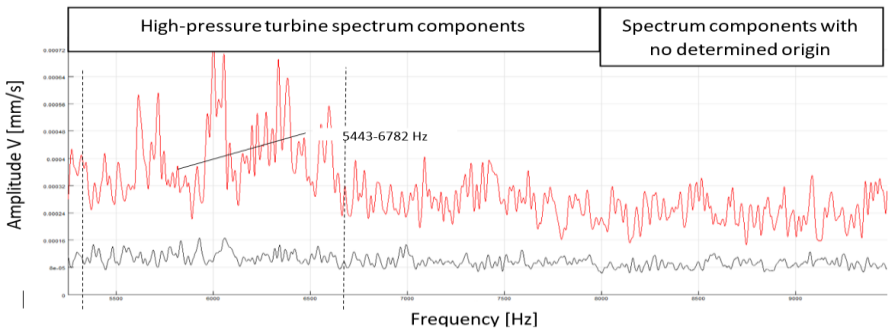

Figure 18. Vibration analysis point no. 4 (bearing no. 5) for the relevant frequency ranges 5–10 kHz.

Based on the readout values of the vibration spectrum components and relating them to the analytically calculated [50] vibration frequencies of the individual engine components, a certain regularity in the spread of damage could be observed (Figure 19).

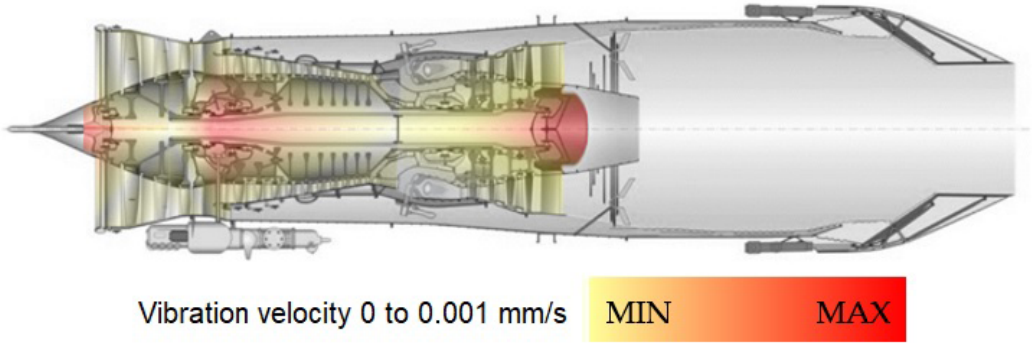

Figure 19. Illustration of vibration energy propagation in the F100-PW-229 engine structure based on the manufacturer's technical documentation.

5. Conclusions

This study provides a detailed vibroacoustic evaluation of the Pratt & Whitney F100-PW-229 jet engine using non-contact laser measurement techniques and Fourier-based spectral decomposition. The results confirm that Fast Fourier Transform (FFT) analysis, when applied to high-resolution vibration data obtained from strategically selected engine locations, offers a robust diagnostic methodology for identifying internal mechanical faults.

- Key findings demonstrate that elevated amplitude components at harmonics of shaft rotational frequencies are strongly correlated with rotor imbalance and bearing degradation particularly at supports 1 and 2. Analytical predictions of characteristic frequencies

associated with various damage modes (e.g., rolling element faults, raceway defects, and cage anomalies) were substantiated by empirical spectral data, establishing high congru-ence between theoretical models and experimental measurements.

- Additionally, propagation patterns of vibrational energy reveal that bearing-induced oscillatory disturbances are transmitted to rotor blade assemblies, amplifying structural responses in the compressor and turbine stages. These interactions potentially compro-mise the integrity of blade mountings and disc-shaft couplings over time, underscoring the necessity of holistic system-level diagnostics.
- The application of laser Doppler vibrometry enabled remote, non-intrusive measurement of structural vibrations with high spatial flexibility, eliminating the constraints asso-ciated with traditional contact-based sensing. This not only enhanced measurement safety and efficiency but also permitted the creation of detailed vibration maps across the en-gine's architecture.
- This study further introduces a methodological framework for vibration signal pro-cessing that combines time- and frequency-domain analysis with feature selection tech-niques such as Relief-F. This lays the groundwork for future integration of machine learn-ing models for condition classification, anomaly detection, and predictive maintenance.

In conclusion, the presented methodology proves effective for detecting and localizing mechanical irregularities in high-performance jet engines. It supports the establishment of a national diagnostic reference database for the F100-PW-229 engine series, which is espe-cially critical given limited access to proprietary OEM diagnostic platforms. The findings advocate for the formal adoption of advanced spectral diagnostics, including laser-based sensing, as part of standardized test-bench procedures aimed at enhancing operational readiness and extending engine service life.

Author Contributions: Conceptualization, W.P.; methodology, W.P., A.M. and B.C.; formal analysis, W.P., A.M. and B.C.; investigation, W.P., A.M. and B.C.; resources, W.P., A.M., B.C. and P.W.S.; data curation, W.P., A.M., B.C., T.G. and P.W.S.; writing—original draft preparation, W.P., A.M., B.C., T.G. and P.W.S.; writing—review and editing, W.P., A.M., B.C., T.G. and P.W.S.; project administration, W.P.; funding acquisition, W.P.; All authors have read and agreed to the published version of the manuscript.

Funding: This work was published with the help of a grant from the Polish Ministry of Education and Science as a statutory activity of the Institute of Structural Analysis under the number 0411/SBAD/0010. This research was funded by the Poznan University of Technology's financial resources for statutory activity, grant numbers 0712/SBAD/5252 and 0712/SBAD/5280.

Data Availability Statement: Data are contained within the article.

Acknowledgments: We would like to extend our sincere thanks to EC TEST Systems Ltd. for generously providing the vibration equipment used in this study. This support contributed to the successful completion of our research.

Conflicts of Interest: The authors declare no conflicts of interest.

References

1. Szczeciński, S.; Balicki, W.J.; Chachurski, R.; Głowacki, P.; Kawalec, K.; Kozakiewicz, A.; Szczeciński, J. *Aerial Power Units*; WAT Publishing House: Warsaw, Poland, 2016; p. 242.
2. Allouis, C.; Amoresano, A.; Quaremba, G.; Langella, G. Analysis of HEFA's Impact on Micro Gas Turbine Emissions and Performances by Nonlinear Vibrational Signatures. *Appl. Therm. Eng.* **2025**, *276*, 126925. [CrossRef]
3. Bu, H.; Huang, X.; Zhang, X. An Overview of Testing Methods for Aeroengine Fan Noise. *Prog. Aerosp. Sci.* **2021**, *124*, 100722. [CrossRef]

4. Vignat, G.; Brouzet, D.; Bonanni, M.; Ihme, M. Analysis of Weak Secondary Waves in a Rotating Detonation Engine Using Large-Eddy Simulation and Wavenumber-Domain Filtering. *Combust. Flame* **2024**, *263*, 113387. [CrossRef]
5. Ahmed, U.; Ali, F.; Jennions, I. A Review of Aircraft Auxiliary Power Unit Faults, Diagnostics and Acoustic Measurements. *Prog. Aerosp. Sci.* **2021**, *124*, 100721. [CrossRef]
6. Moghadam, F.K.; Nejad, A.R. Theoretical and Experimental Study of Wind Turbine Drivetrain Fault Diagnosis by Using Torsional Vibrations and Modal Estimation. *J. Sound Vib.* **2021**, *509*, 116223. [CrossRef]
7. Rego, L.; Avallone, F.; Ragni, D.; Casalino, D. On the Mechanisms of Jet-Installation Noise Reduction with Flow-Permeable Trailing Edges. *J. Sound Vib.* **2022**, *520*, 116582. [CrossRef]
8. Chen, G.; Alam, M.M.; Zhou, Y.; Ji, C.; Zhu, H. Wall-Proximity Effects on Vortex-Induced Vibrations of a Circular Cylinder. *Ocean Eng.* **2023**, *287*, 115874. [CrossRef]
9. Rokicki, E.; Gradzki, R.; Kulesza, Z.; Cecotka, P.; Dec, K. Frequency and Modeshape Evaluation of Steam Turbine Blades Using the Metal Magnetic Memory Method and Vibration Wave Propagation. *Mech. Syst. Signal Process.* **2023**, *192*, 110218. [CrossRef]
10. Ren, R.; Ma, X.; Yue, H.; Yang, F.; Lu, Y. Stiffness Enhancement Methods for Thin-Walled Aircraft Structures: A Review. *Thin-Walled Struct.* **2024**, *201*, 111995. [CrossRef]
11. Chu, T.; Nguyen, T.; Yoo, H.; Wang, J. A Review of Vibration Analysis and Its Applications. *Heliyon* **2024**, *10*, e26282. [CrossRef]
12. Fahmi, A.-T.W.K.; Kashyzadeh, K.R.; Ghorbani, S. A Comprehensive Review on Mechanical Failures Cause Vibration in the Gas Turbine of Combined Cycle Power Plants. *Eng. Fail. Anal.* **2022**, *134*, 106094. [CrossRef]
13. Xie, J.; Liu, J.; Chen, J.; Zi, Y. Blade Damage Monitoring Method Based on Frequency Domain Statistical Index of Shaft's Random Vibration. *Mech. Syst. Signal Process.* **2022**, *165*, 108351. [CrossRef]
14. Kumar, P.; Tiwari, R. Additive fault diagnosis techniques in rotor systems: A state-of-the-art review. *Sādhanā* **2024**, *49*, 207. [CrossRef]
15. Djaidir, B.; Hafaifa, A.; Kouzou, A. Faults detection in gas turbine rotor using vibration analysis under varying conditions. *J. Theor. Appl. Mech.* **2017**, *55*, 393–406. [CrossRef]
16. Greiffenhagen, F.; Peterleithner, J.; Woisetschläger, J. Prediction of combustion noise of a swirl-stabilized flame using laser interferometric vibrometry validated by acoustic measurements. In Proceedings of the ASME Turbo Expo, Charlotte, NC, USA, 26–30 June 2017. [CrossRef]
17. Greiffenhagen, F.; Woisetschläger, J.; Gürtler, J.; Czarske, J. Quantitative measurement of density fluctuations with a full-field laser interferometric vibrometer. *Exp. Fluids* **2020**, *61*, 1. [CrossRef]
18. Jia, H.; Zhang, Q.; Wei, M.; Sun, X. Sparse Fast Fourier Transform analysis of aero-engine vibration data. *J. Phys. Conf. Ser.* **2024**, *2762*, 012036. [CrossRef]
19. Tama, B.A.; Vania, M.; Lee, S.; Lim, S. Recent advances in the application of deep learning for fault diagnosis of rotating machinery using vibration signals. *Artif. Intell. Rev.* **2023**, *56*, 4667–4709. [CrossRef]
20. Prokopowicz, W. Detection of Cracks In Composite Materials Using Hybrid Non-Destructive Testing Method Based on Vibro-Thermography and Time-Frequency Analysis of Ultrasonic Excitation Signal. *J. KONBIN* **2015**, *2*, 71–86. [CrossRef]
21. Guminiak, M.; Knitter-Piatkowska, A. Selected problems of damage detection in internally supported plates using one-dimensional discrete wavelet transform. *J. Theor. Appl. Mech.* **2018**, *56*, 631–644. [CrossRef]
22. Nowakowski, T.; Komorski, P. Diagnostics of the drive shaft bearing based on vibrations in the high-frequency range as a part of the vehicle's self-diagnostic system. *Eksploat. Niezawodn.—Maint. Reliab.* **2022**, *24*, 70–79. [CrossRef]
23. Tabaszewski, M.; Szymański, G.M.; Nowakowski, T. Vibration-based identification of engine valve clearance using a convolutional neural network. *Arch. Transp.* **2022**, *61*, 117–131. [CrossRef]
24. Nowakowski, T.; Tomaszewski, F.; Komorski, P.; Szymański, G.M. Tram gearbox condition monitoring method based on trackside acoustic measurement. *Measurement* **2023**, *207*, 112358. [CrossRef]
25. Grądzki, R.; Lindstedt, P.; Bartoszewicz, B.; Kulesza, Z. Assessment of rotor blades stationarity condition based on differences in phase shifts. *Eng. Fail. Anal.* **2020**, *118*, 104874. [CrossRef]
26. Pludra, A.; Przybylski, M. Experimental measurement of the bullet trajectory after perforation of a chambered window. *Int. J. Appl. Glass Sci.* **2019**, *10*, 441–448. [CrossRef]
27. Prokopowicz, W. Study of the vibroacoustic response of the composite structure of the wing of the FALRIS LAR 1 aircraft in terms of damage localization. In *Aviation for Defence*; 2 Skrzydło Lotnictwa Taktycznego: Poznań, Poland, 2016; ISBN 978-83-7775-428-3.
28. Prokopowicz, W. A new approach to damage detection in composite materials using a hybrid non-destructive testing method. *J. Mech. Transp. Eng.* **2016**, *68*, 2.
29. Sumelka, W.; Nowak, M.; Nassr, A.A.; Studziński, R.; Sielicki, P.W. Dynamic failure of the aluminium plate under air-blast loading in the framework of the fractional viscoplasticity model—Theory and validation. *Int. J. Impact Eng.* **2021**, *158*, 104024. [CrossRef]
30. Studziński, R.; Gajewski, T.; Malendowski, M.; Sumelka, W.; Al-Rifaie, H.; Peksa, P.; Sielicki, P.W. Blast test and failure mechanisms of soft-core sandwich panels for storage halls applications. *Materials* **2020**, *14*, 70. [CrossRef]

31. Tang, N.; Zhang, B.; Lord, C.; Marshall, M. Identification of blade operational mode shapes during wear of abradable coating. *J. Sound Vib.* **2020**, *472*, 115204. [CrossRef]
32. Lockheed Martin. *Customer Training Student Training Manual, STP 16-329PL Revision Orig. Volume I, F100-PW-229 Power Plant (Poland Block 52)*; Lockheed Martin: Bethesda, MD, USA, 2006.
33. Cempel, C. *Applied Vibroacoustics*; PWN Publishing House: Warsaw, Poland, 1978; p. 58.
34. Clifton, D. *Condition Monitoring of Gas-Turbine Engines*; St. Cross College, Department of Engineering Science, University of Oxford: Oxford, UK, 2006; p. 15.
35. Fabry, S.; Ceskovic, M. Aircraft gas turbine engine vibration diagnostic. *Mag. Avia. Dev.* **2017**, *5*, 24–28. [CrossRef]
36. Moczko, J.; Kramer, L. *Digital Methods of Biomedical Signal Processing*; UAM Publishing House: Poznań, Poland, 2001; pp. 168–171.
37. Kotlarz, W.; Królik, M.; Kolasa, R. Influence of modular F100-PW-229 engine construction upon the fleet of F-16 aircraft exploitation. *J. Polish CIMAC* **2014**. Available online: https://yadda.icm.edu.pl/baztech/element/bwmeta1.element.baztech-5ab57c18-6f34-4eb5-9a62-8485a2c123a1/c/CIMAC_2014_9_3_002.pdf (accessed on 1 November 2024).
38. Dowling, P.; Mahmoudi, Y. Combustion noise. *Proc. Combust. Inst.* **2015**, *35*, 65–100. [CrossRef]
39. Szczeciński, S.; Balicki, W. Vibration of turbine engines as the criterion of production quality of rotor assemblies and their current technical state. *Trans. Aerosp. Res.* **2005**, *183*, 173–181.
40. FEDLOG—Federal Logistics—Database of Spare Parts for Aerospace Technology Equipment Manufactured in the United States. Available online: https://www.dla.mil/Information-Operations/Services/Applications/FED-LOG/ (accessed on 1 November 2024).
41. Maynard, K.; Trethewey, M. Blade and shaft crack detection using torsion vibration measurement part 3: Field application demonstrations. *Noise Vib. Worldw.* **2001**, *32*, 16–23. [CrossRef]
42. Cempel, C. *Fundamentals of Vibroacoustic Machine Diagnostics*; WNT: Warsaw, Poland, 1982; pp. 230–242.
43. Eshleman, R.L.; Lewis, F.M. Torsional vibration in reciprocating and rotating machines. In *Shock and Vibration Handbook*; McGraw-Hill: New York, NY, USA, 1988.
44. Gubran. Vibration Diagnosis of Blades of Rotating Machines. Ph.D. Thesis, University of Manchester, Manchester, UK, 2015; p. 49.
45. Al-Bedoor, B. Dynamic model of coupled shaft torsional and blade bending deformations in rotors. *Comput. Methods Appl. Mech. Eng.* **1999**, *169*, 177–190. [CrossRef]
46. Yang, H.; Huang, S.C. The coupled vibration in a shaft-disk-blades system. *J. Chin. Inst. Eng.* **2005**, *28*, 89–99. [CrossRef]
47. Yang, H.; Huang, S.C. The influence of disk's flexibility on coupling vibration of shaft-disk-blades systems. *J. Sound Vib.* **2007**, *301*, 1–17. [CrossRef]
48. Huang, S.; Ho, K. Coupled shaft-torsion and blade-bending vibrations of a rotating shaft-disk-blade unit. *J. Eng. Gas Turbines Power* **1996**, *118*, 100–106. [CrossRef]
49. Al-Bedoor, B. Reduced-order nonlinear dynamic model of coupled shaft-torsional and blade-bending vibrations in rotors. *J. Eng. Gas Turbines Power* **2001**, *123*, 82–88. [CrossRef]
50. Cempel, C. *Vibroacoustic Diagnostics of Machines*; PWN: Warsaw, Poland, 1989; pp. 110–121.